

Colossal barocaloric effects in the complex hydride $\text{Li}_2\text{B}_{12}\text{H}_{12}$

Kartik Sau,¹ Tamio Ikeshoji,¹ Shigeyuki Takagi,² Shin-ichi Orimo,^{2,3} Daniel Errandonea,⁴ Dewei Chu,⁵ and Claudio Cazorla^{5,*}

¹*Mathematics for Advanced Materials - Open Innovation Laboratory (MathAM-OIL), National Institute of Advanced Industrial Science and Technology (AIST), c/o Advanced Institute of Material Research (AIMR), Tohoku University, Sendai 980-8577, Japan*

²*Institute for Materials Research, Tohoku University, Sendai 980-8577, Japan*

³*Advanced Institute for Materials Research, Tohoku University, Sendai 980-8577, Japan*

⁴*Departament de Física Aplicada, Institut de Ciència de Materials, MALTA Consolider Team, Universitat de València, Edifici d'Investigació, Burjassot 46100, Spain*

⁵*School of Materials Science and Engineering, UNSW Sydney, NSW 2052, Australia*

Traditional refrigeration technologies based on compression cycles of greenhouse gases pose serious threats to the environment and cannot be downscaled to electronic device dimensions. Solid-state cooling exploits the thermal response of caloric materials to external fields and represents a promising alternative to current refrigeration methods. However, most of the caloric materials known to date present relatively small adiabatic temperature changes ($|\Delta T| \sim 1$ K) and/or limiting irreversibility issues resulting from significant phase-transition hysteresis. Here, we predict the existence of colossal barocaloric effects (isothermal entropy changes of $|\Delta S| \sim 100 \text{ JK}^{-1}\text{kg}^{-1}$) in the energy material $\text{Li}_2\text{B}_{12}\text{H}_{12}$ by means of molecular dynamics simulations. Specifically, we estimate $|\Delta S| = 387 \text{ JK}^{-1}\text{kg}^{-1}$ and $|\Delta T| = 26 \text{ K}$ for an applied pressure of $P = 0.4 \text{ GPa}$ at $T = 475 \text{ K}$. The disclosed colossal barocaloric effects are originated by an order-disorder phase transformation that exhibits a fair degree of reversibility and involves coexisting Li^+ diffusion and $(\text{BH})_{12}^{2-}$ reorientational motion at high temperatures.

Solid-state cooling is an environmentally friendly, energy efficient, and highly scalable technology that can solve most of the problems associated with conventional refrigeration methods based on compression cycles of greenhouse gases (i.e., environmental harm and lack of downsize scaling). Upon application of magnetic, electric or stress fields good caloric materials undergo noticeable temperature changes ($|\Delta T| \sim 1\text{--}10 \text{ K}$) as a result of induced phase transformations that involve large entropy variations ($|\Delta S| \sim 10\text{--}100 \text{ JK}^{-1}\text{kg}^{-1}$) [1–3]. Solid-state cooling capitalizes on such caloric effects to engineer refrigeration cycles. From a performance point of view, that is, largest $|\Delta T|$ and $|\Delta S|$ (although these are not the only parameters defining cooling efficiency [4]), barocaloric effects driven by small hydrostatic pressure shifts appear to be the most promising [1–3].

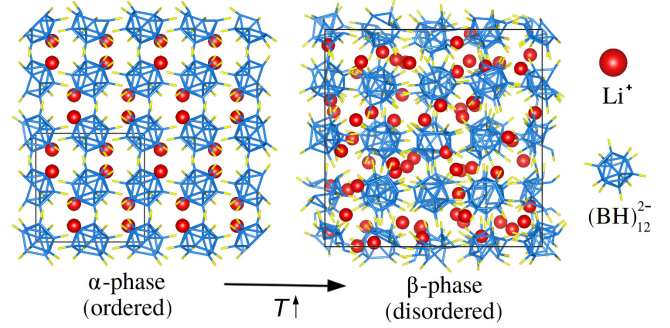


FIG. 1. Low- T (ordered) and high- T (disordered) phases of bulk $\text{Li}_2\text{B}_{12}\text{H}_{12}$. The low- T phase (α) presents cubic symmetry and space group $P\bar{a}3$ [15]. In the high- T phase (β), cubic symmetry is preserved but the Li^+ ions are highly mobile and the $(\text{BH})_{12}^{2-}$ icosahedra present reorientational disorder [18]. The T -induced $\alpha \rightarrow \beta$ phase transition is an order-disorder isosymmetric transformation [18]. Li, B, and H ions are represented with red, blue, and yellow colours, respectively.

Recently, colossal barocaloric effects (defined here as $|\Delta S| \sim 100 \text{ JK}^{-1}\text{kg}^{-1}$) have been measured in two different families of materials that display intriguing order-disorder phase transitions [5–7]. First, giant barocaloric effects have been theoretically predicted [8] and experimentally observed in the archetypal superionic compound AgI [5]. AgI exhibits a first-order normal (low-entropy) to superionic (high-entropy) phase transition that responds to both temperature and pressure [9] and which involves the presence of highly mobile silver ions in the high- T superionic state [10]. The entropy changes estimated for other normal to superionic phase transitions in general are large as well [11–14]. And second, colossal barocaloric effects have been reported for the molecular solid neopentylglycol [6, 7], $(\text{CH}_3)_2\text{C}(\text{CH}_2\text{OH})_2$, and other plastic crystals [4]. In these solids molecules reorient almost freely around their centers of mass, which remain localized at well-defined lattice positions. Molecular rotations lead to orientational disorder, which renders high entropy. By using hydrostatic pressure, it is possible to block such molecular reorientational motion and thus induce a fully ordered state characterized by low entropy [14]. The barocaloric effects resulting from

* Corresponding Author

this class of order-disorder phase transition are huge and comparable in magnitude to those achieved in conventional refrigerators with environmentally harmful fluids [4, 6, 7].

Here, we report the prediction of colossal barocaloric effects ($|\Delta S| \sim 100 \text{ JK}^{-1}\text{kg}^{-1}$) in the energy material $\text{Li}_2\text{B}_{12}\text{H}_{12}$ (LBH), a complex hydride that is already known from the fields of hydrogen storage [15–17] and solid-state batteries [18–20]. By using molecular dynamics simulations, we identify a pressure-induced isothermal entropy change of $|\Delta S| = 387 \text{ JK}^{-1}\text{kg}^{-1}$ and adiabatic temperature change of $|\Delta T| = 26 \text{ K}$ at $T = 475 \text{ K}$. These colossal entropy and temperature changes are driven by moderate hydrostatic pressure shifts of $P = 0.4 \text{ GPa}$, thus yielding huge barocaloric strengths of $|\Delta S|/P = 968 \text{ JK}^{-1}\text{kg}^{-1}\text{GPa}^{-1}$ and $|\Delta T|/P = 65 \text{ K GPa}^{-1}$. The colossal barocaloric effects disclosed in bulk LBH are originated by simultaneous P -driven frustration and activation of Li^+ diffusion and $(\text{BH})_{12}^{-2}$ icosahedra reorientational motion. Thus, alkali-metal complex borohydrides ($\text{A}_2\text{B}_{12}\text{H}_{12}$, $\text{A} = \text{Li, Na, K, Cs}$ [21, 22]) emerge as a promising new family of barocaloric materials in which the salient phase-transition features of fast-ion conductors and plastic crystals coexist.

RESULTS

At ambient conditions, lithium dodecahydrododecaborate ($\text{Li}_2\text{B}_{12}\text{H}_{12}$), LBH, presents an ordered cubic $Pa\bar{3}$ phase, referred to as α hereafter, which is characterized by Li^+ cations residing on near-trigonal-planar sites surrounded by three $(\text{BH})_{12}^{-2}$ icosahedron anions. In turn, each $(\text{BH})_{12}^{-2}$ anion resides in an octahedral cage surrounded by six Li^+ cations (Fig.1a) [15]. A symmetry preserving order-disorder phase transition occurs at high temperatures ($\sim 500 \text{ K}$) that stabilises a disordered state, referred to as β hereafter, in which the Li^+ cations are mobile and the $(\text{BH})_{12}^{-2}$ anions present reorientational motion (Fig.1b) [18]. The relative volume expansion that has been experimentally measured for such an order-disorder phase transition is $\approx 8\%$ [18]. This huge volume variation along with the accompanying, and presumably also large, phase-transition entropy change could be propitious for barocaloric purposes if the involved phase transformation was responsive to moderate external pressures of $\sim 0.1 \text{ GPa}$. To the best of our knowledge, this possibility has not been hitherto explored. We performed classical molecular dynamics (MD) simulations based on a recently proposed LBH force field [23] to fill up such a knowledge gap (Methods and Supplementary Methods), which has clear implications for potential solid-state cooling applications.

Figure 2a shows the P - T phase diagram that we estimated for bulk LBH using atomistic MD simulations. It was found that the temperature of the $\alpha \rightarrow \beta$ phase transition is certainly sensitive to external pressure. Specifically, the dP/dT derivative of the corresponding phase

boundary amounts to $\approx 0.008 \text{ GPa K}^{-1}$ at zero pressure and to $\approx 0.02 \text{ GPa K}^{-1}$ at $P = 0.2 \text{ GPa}$. Likewise, the relative volume change ascribed to the $\alpha \rightarrow \beta$ transformation is, according to our simulations, $+4.6\%$ at zero pressure and $+3.4\%$ at $P = 0.2 \text{ GPa}$ (Fig.2b). By using these thermodynamic data and the Clausius-Clapeyron relation [2], we roughly estimated an entropy change of $\Delta S \sim 300 \text{ JK}^{-1}\text{kg}^{-1}$ for the order-disorder transition occurring in LBH at $P = 0.2 \text{ GPa}$. In view of these promising barocaloric descriptor values, we proceeded to accurately calculate the barocaloric isothermal entropy and adiabatic temperature changes, ΔS and ΔT , induced by pressures $0 \leq P \leq 0.4 \text{ GPa}$. To this end, we followed the numerical protocols described in the Methods section, which essentially involve the determination of the volume and heat capacity of bulk LBH (Fig.2c) as a function of pressure and temperature.

The results of our precise barocaloric calculations for temperatures and pressures in the intervals $450 \leq T \leq 525 \text{ K}$ and $0 \leq P \leq 0.4 \text{ GPa}$ are shown in Figs. 2d,e. The ΔS and ΔT values estimated for the $\alpha \rightarrow \beta$ transformation in fact render colossal barocaloric effects. For example, at $T = 490 \text{ K}$ and $P = 0.4 \text{ GPa}$ (0.2 GPa) we calculated an isothermal entropy change of $-365 \text{ JK}^{-1}\text{kg}^{-1}$ ($-135 \text{ JK}^{-1}\text{kg}^{-1}$) and an adiabatic temperature change of $+27 \text{ K}$ ($+10 \text{ K}$). The resulting barocaloric effects are direct, that is, $\Delta T > 0$, because the low-entropy ordered state is stabilized under pressure ($\Delta S < 0$). A maximum $|\Delta S|$ value of $387 \text{ JK}^{-1}\text{kg}^{-1}$ was found at $T = 475 \text{ K}$ and $P = 0.4 \text{ GPa}$ (Fig.2d). For temperatures above $\approx 510 \text{ K}$, we estimated noticeably smaller $|\Delta S|$ and ΔT values (e.g., $72 \text{ JK}^{-1}\text{kg}^{-1}$ and 10 K for $P = 0.4 \text{ GPa}$ at $T = 525 \text{ K}$), a trend that we link to some anomalous pressure-induced ionic diffusion (explained below). In the Discussion section, we will compare the barocaloric performance of LBH with those of other well-known barocaloric materials. In what follows, the atomistic mechanisms leading to the extraordinary ΔS and ΔT results just reported are unravelled.

There are two possible sources of large entropy variation in LBH, one stemming from the Li^+ ionic diffusion and the other from the $(\text{BH})_{12}^{-2}$ icosahedra reorientational motion. When hydrostatic pressure is applied on the disordered β phase at temperatures below $\approx 500 \text{ K}$, both the ionic diffusion and molecular orientational disorder are reduced and thus the crystal entropy diminishes significantly. This conclusion is straightforwardly deduced from the P -induced variation of the Li^+ diffusion coefficient, D_{Li} , and reorientational $(\text{BH})_{12}^{-2}$ frequency, $\lambda_{\text{B}_{12}\text{H}_{12}}$, shown in Figs.3a,b (Methods). For instance, at $T = 475 \text{ K}$ and zero pressure D_{Li} and $\lambda_{\text{B}_{12}\text{H}_{12}}$ amount to $2.5 \cdot 10^{-6} \text{ cm}^2\text{s}^{-1}$ and $1.2 \cdot 10^8 \text{ s}^{-1}$, respectively, whereas at $P = 0.2 \text{ GPa}$ both quantities are practically zero (Fig.3). The two resulting contributions to the system entropy variation are of the same sign and make $|\Delta S|$ huge.

Which of these two P -induced order-restoring effects is most relevant for the barocaloric performance of bulk LBH? To answer this question, we performed constrained

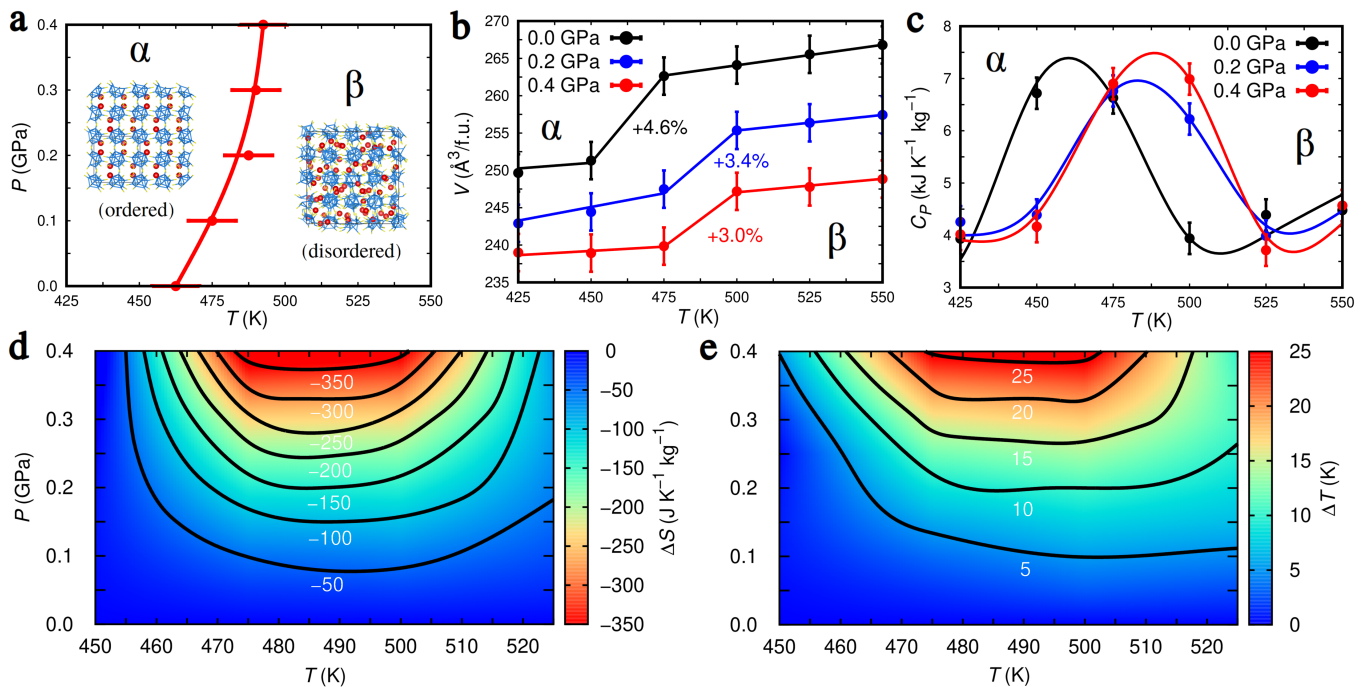


FIG. 2. Influence of pressure on the T -induced $\alpha \rightarrow \beta$ phase transition occurring in bulk $\text{Li}_2\text{B}_{12}\text{H}_{12}$ and the resulting barocaloric effects. **a** Estimated P - T phase boundary separating the stability regions of the α and β phases. **b** Volume change estimated for the T -induced $\alpha \rightarrow \beta$ phase transition at different pressures. **c** Heat capacity of bulk $\text{Li}_2\text{B}_{12}\text{H}_{12}$ expressed as a function of temperature and pressure. **d** Isothermal entropy and **e** adiabatic temperature changes associated with the barocaloric response of bulk $\text{Li}_2\text{B}_{12}\text{H}_{12}$ expressed as a function of applied pressure and temperature. Solid black lines represent isovalue curves.

MD simulations in which we forced the Li^+ ions to remain localized around their equilibrium positions independently of temperature. This type of artificial condition in principle cannot be imposed in the experiments but can be easily enforced in the atomistic simulations. The $|\Delta S|$ values estimated in these constrained MD simulations were roughly half the value of the isothermal entropy changes obtained in the standard MD simulations. Therefore, we may conclude that at temperatures below ≈ 500 K the pressure-induced entropy changes stemming from the Li^+ ionic diffusion and $(\text{BH})_{12}^{-2}$ icosahedra reorientational motion variations play both an equally important role in the global barocaloric response of LBH.

Figure 3a shows that at $T \gtrsim 500$ K the Li^+ diffusion coefficient increases under increasing pressure. For example, at $T = 525$ K and zero pressure we estimate $D_{\text{Li}} = 8.7 \cdot 10^{-6} \text{ cm}^2\text{s}^{-1}$ whereas at $P = 0.4$ GPa and the same temperature we obtain $17.2 \cdot 10^{-6} \text{ cm}^2\text{s}^{-1}$. This ionic diffusion behaviour is highly anomalous because hydrostatic compression typically hinders ionic transport [9–11]. On the other hand, the reorientational motion of the $(\text{BH})_{12}^{-2}$ icosahedra behaves quite normally, that is, decreases under pressure [3, 4]. For instance, at $T = 525$ K and zero pressure we estimate $\lambda_{\text{B}_{12}\text{H}_{12}} = 1.4 \cdot 10^8 \text{ s}^{-1}$ whereas at $P = 0.4$ GPa and the same temperature we obtain $0.7 \cdot 10^8 \text{ s}^{-1}$ (Fig.3b). We hypothesize that the anomalous P -induced Li^+ diffusion behaviour observed in our MD simulations is due to the high anionic reorientational

motion, which makes the $(\text{BH})_{12}^{-2}$ centers of mass to fluctuate and partially block the ionic current channels [24]. Consistently, when the frequency of the $(\text{BH})_{12}^{-2}$ rotations is reduced by effect of compression the ions can flow more easily throughout the crystal and Li^+ transport is enhanced. In this particular P - T region, the two contributions to the crystal entropy variation stemming from Li^+ ionic diffusion and $(\text{BH})_{12}^{-2}$ icosahedra reorientational motion have opposite signs hence $|\Delta S|$ decreases significantly. The identified anomalous lithium diffusion behaviour, however, ceases at $P \approx 0.6$ GPa since beyond that point D_{Li} decreases systematically upon increasing pressure (Supplementary Fig.1).

DISCUSSION

To date, large BC effects have been experimentally measured for a number of shape-memory alloys [25, 26], polar compounds [27], organic-inorganic hybrid perovskites [28, 29], fluoride-based materials [30], polymers [31], the fast-ion conductor AgI [5] and molecular crystals [6, 7, 32]. In Table I, we compare the barocaloric performance predicted for bulk LBH with those of some representative barocaloric materials [1–3]. The isothermal entropy change induced in LBH by a moderate hydrostatic pressure of 0.4 GPa, $387 \text{ JK}^{-1}\text{kg}^{-1}$, is comparable in magnitude to the record $|\Delta S|$ that has been

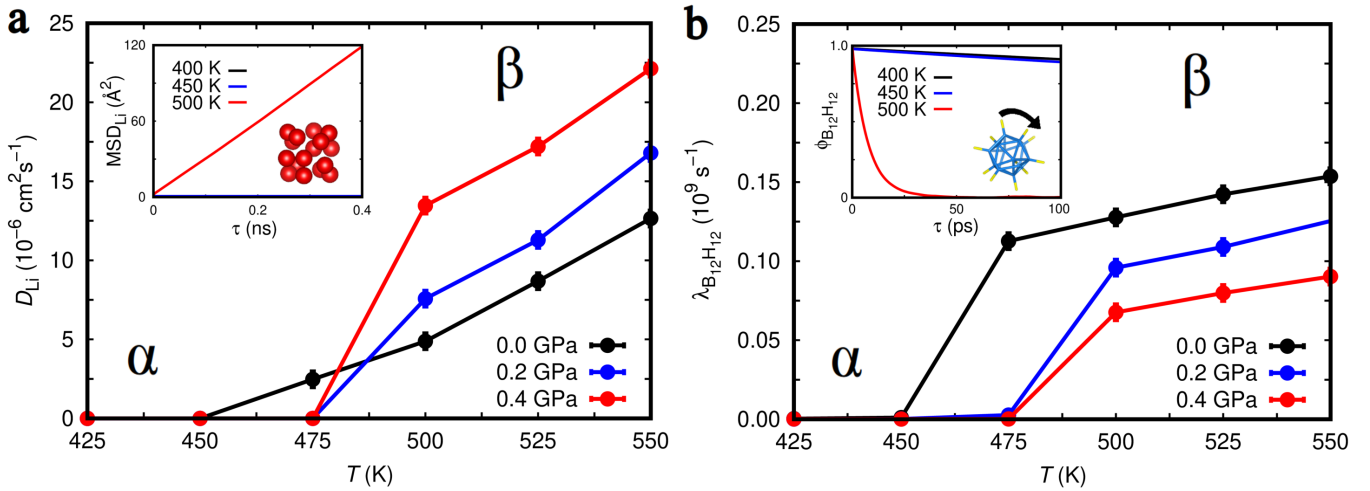


FIG. 3. Order parameter changes associated with the T -induced $\alpha \rightarrow \beta$ phase transition occurring in bulk $\text{Li}_2\text{B}_{12}\text{H}_{12}$ at different pressures. **a** Estimated lithium ion diffusion coefficient, D_{Li} , expressed as a function of temperature and pressure. The inset shows the Li mean-squared displacement (MSD_{Li}) data employed for the calculation of D_{Li} at zero pressure (Methods). **b** Estimated $(\text{BH})_{12}^{-2}$ icosahedra reorientational rate, $\lambda_{\text{B}_{12}\text{H}_{12}}$, expressed as a function of temperature and pressure. The inset shows the $(\text{BH})_{12}^{-2}$ icosahedra angular auto-correlation function ($\phi_{\text{B}_{12}\text{H}_{12}}$) data employed for the calculation of $\lambda_{\text{B}_{12}\text{H}_{12}}$ at zero pressure (Methods).

	T (K)	P (GPa)	$ \Delta S $ ($\text{JK}^{-1}\text{kg}^{-1}$)	$ \Delta T $ (K)	$ \Delta S /P$ ($\text{JK}^{-1}\text{kg}^{-1}\text{GPa}^{-1}$)	$ \Delta T /P$ (K GPa^{-1})	Material	Reference
$\text{Ni}_{51}\text{Mn}_{33}\text{In}_{16}$	330	0.25	41.0	4.0	164	16.0	SMA	[25]
$\text{Fe}_{49}\text{Rh}_{51}$	310	0.11	12.5	8.1	114	73.6	SMA	[26]
$(\text{NH}_4)_2\text{SO}_4$	220	0.10	130.0	8.0	1300	80.0	FE	[27]
$[\text{TPrA}][\text{Mn}(\text{dca})_3]$	330	0.01	30.5	4.1	3050	410.0	OIH	[28]
$[\text{FeL}_2][\text{BF}_4]_2$	262	0.03	80.0	3.0	2667	100.0	MC	[32]
$(\text{CH}_3)_2\text{C}(\text{CH}_2\text{OH})_2$	320	0.52	510.0	45.0	981	86.5	MC	[6, 7]
AgI	400	0.25	62.0	36.0	248	144.0	FIC	[5]
$\text{Li}_2\text{B}_{12}\text{H}_{12}$	475	0.40	387.0	26.0	968	65.0	FIC/MC	This work

TABLE I. Materials presenting giant ($|\Delta S| \sim 10 \text{ JK}^{-1}\text{kg}^{-1}$) and colossal ($\sim 100 \text{ JK}^{-1}\text{kg}^{-1}$) barocaloric effects. T represents working temperature, P applied pressure, $|\Delta S|$ isothermal entropy change, $|\Delta T|$ adiabatic temperature change, $|\Delta T|/P$ barocaloric strength, “SMA” shape-memory alloy, “FE” ferroelectric, “OIH” organic-inorganic hybrid perovskite, “MC” molecular crystal and “FIC” fast-ion conductor.

recently reported for the plastic crystal neopentylglycol by considering a similar pressure shift, $510 \text{ JK}^{-1}\text{kg}^{-1}$ [6, 7]. The rest of materials in Table I present isothermal entropy changes that are appreciably smaller, made the exception of the polar crystal $(\text{NH}_4)_2\text{SO}_4$ which registers $130 \text{ JK}^{-1}\text{kg}^{-1}$. As regards $|\Delta T|$, the clear contestants of LBH are the fast-ion conductor AgI (36 K) and again the plastic crystal $(\text{CH}_3)_2\text{C}(\text{CH}_2\text{OH})_2$ (45 K). The reason for the smaller $|\Delta T|$ value estimated for LBH as compared to that of AgI is the significantly larger heat capacity of the former material, which results from a smaller molecular weight [12]. In terms of the barocaloric strengths defined as $\text{BSS} \equiv |\Delta S|/P$ and $\text{BST} \equiv |\Delta T|/P$, LBH remains competitive with the best performers.

For instance, the organic-inorganic hybrid perovskite $[\text{TPrA}][\text{Mn}(\text{dca})_3]$ displays the largest BSS and BST coefficients of all crystals, $\approx 3,000 \text{ JK}^{-1}\text{kg}^{-1}\text{GPa}^{-1}$ and $\approx 400 \text{ K GPa}^{-1}$, respectively, while for bulk LBH we estimate $\approx 1,000 \text{ JK}^{-1}\text{kg}^{-1}\text{GPa}^{-1}$ and $\approx 100 \text{ K GPa}^{-1}$. Meanwhile, the barocaloric strengths reported for the plastic crystal neopentylglycol are comparable in magnitude to those predicted for LBH, which hints at their common order-disorder phase-transition origin.

As it was mentioned in the Introduction, the magnitude of the $|\Delta T|$ and $|\Delta S|$ shifts are not the only parameters that define the barocaloric performance of a material. The degree of reversibility of the involved P -induced phase transition, for instance, is another impor-

tant barocaloric descriptor that provides information on the materials efficiency during successive pressure application/removal cycles. Specifically, the hysteresis of the transition makes the materials behaviour to depend on its cycling history and to increase the value of the external field that is required to bring the phase transition to completion [4]. As a consequence, the barocaloric performance of a hysteretic material can be significantly worse than that of its ideal non-hysteretic counterpart. In order to quantify the degree of reversibility associated with the $\alpha \leftrightarrow \beta$ phase transition in LBH, we performed a series of long MD simulations (~ 2 ns) in which the pressure (temperature) was kept fixed while the temperature (pressure) was varied steadily first from 425 up to 625 K (from 0.0 up to 0.4 GPa) and subsequently from 625 back to 425 K (from 0.4 back to 0.0 GPa). The results of such field-changing simulations indicate that the degree of reversibility of the order-disorder $\alpha \rightarrow \beta$ phase transition is quite acceptable (Supplementary Fig.2). For instance, by monitoring the variation of the system volume, we found that at zero pressure the difference between the transition temperatures observed during the heating and cooling stages was $\Delta T_h \equiv T_{\alpha \rightarrow \beta} - T_{\beta \rightarrow \alpha} \approx 50$ K (Supplementary Fig.2a). The size of ΔT_h , however, increases noticeably at higher pressures (≈ 100 K at 0.4 GPa). Meanwhile, at fixed temperature we found that the hysteresis of the phase transition as driven by pressure was practically null at $T = 550$ K ($\Delta P_h \approx 0$ GPa) and equal to 0.1 GPa at 475 K (Supplementary Fig.2b).

Arguably the only weakness of bulk LBH in terms of barocaloric potential is that the critical temperature of the order-disorder $\alpha \rightarrow \beta$ phase transition is significantly higher than room temperature. However, this practical problem can be efficiently solved by means of doping and alloying strategies. In fact, recently it has been experimentally shown that carbon-doped LBH, $\text{LiCB}_{11}\text{H}_{12}$, presents a much lower $\alpha \rightarrow \beta$ transition temperature of ≈ 400 K [33], and that the disordered β phase is already stabilized at room temperature in $\text{Li}(\text{CB}_9\text{H}_{10})\text{-Li}(\text{CB}_{11}\text{H}_{12})$ solid solutions [34]. Moreover, the type of isosymmetric order-disorder phase transition underlying the exceptional barocaloric behaviour of LBH occurs also in analogous alkali-metal complex hydrides ($\text{A}_2\text{B}_{12}\text{H}_{12}$, $\text{A} = \text{Na}, \text{K}, \text{Cs}$) [35] and other earth-abundant and non-toxic materials like KHPO_4 , $\text{NaAlSi}_3\text{O}_8$ and KNO_3 [36]. Bulk KNO_3 , for example, displays a staggering volume collapse of $\sim 10\%$ for a room-temperature phase transformation induced by a modest pressure of 0.3 GPa [37], which suggests great barocaloric potential as well.

In conclusion, we have predicted the existence of colossal barocaloric effects rendering isothermal entropy changes of $\sim 100 \text{ JK}^{-1}\text{kg}^{-1}$ and adiabatic temperature shifts of ~ 10 K in the complex hydride $\text{Li}_2\text{B}_{12}\text{H}_{12}$, which are driven by moderate hydrostatic pressures of ~ 0.1 GPa. The phase transition underlying such colossal barocaloric effects is remarkable as it combines key ingredients of fast-ion conductors (i.e., ionic diffusion) and molecular crystals (i.e., reorientational motion), ma-

terials that individually have been proven to be excellent barocaloric materials. This same type of isosymmetric order-disorder phase transition is likely to occur also in other economically affordable and innocuous compounds (e.g., $\text{Cs}_2\text{B}_{12}\text{H}_{12}$ and KNO_3), thus broadening significantly the spectrum of caloric materials with commercial potential for solid-state cooling applications. We believe that our simulation study will stimulate experimental research on this new family of barocaloric materials, namely, alkali-metal complex hydrides, which are already known from other technological disciplines (e.g., hydrogen storage and electrochemical devices) and are routinely synthesized in the laboratory.

METHODS

Classical molecular dynamics simulations. Molecular dynamics (MD) (N, P, T) simulations were performed with the LAMMPS code [38]. The pressure and temperature in the system were kept fluctuating around a set-point value by using thermostatting and barostatting techniques in which some dynamic variables are coupled to the particle velocities and simulation box dimensions. The interactions between atoms were modeled with the harmonic Coulomb-Buckingham interatomic potential reported in work [23], the details of which are provided in the Supplementary Methods. The employed interatomic potential reproduces satisfactorily the vibrational spectra, structure and lithium diffusion coefficients of bulk LBH [23] (Supplementary Discussion). We employed simulation boxes containing 6656 atoms and applied periodic boundary conditions along the three Cartesian directions. Newton's equations of motion were integrated using the customary Verlet's algorithm with a time-step length of 0.5 fs. The typical duration of a MD (N, P, T) run was of 1 ns. A particle-particle particle-mesh k -space solver was used to compute long-range van der Waals and Coulomb interactions beyond a cut-off distance of 10 Å at each time step.

Density functional theory calculations. First-principles calculations based on density functional theory (DFT) [39] were performed to analyse the energy, structural, vibrational, and ionic transport properties of $\text{Li}_2\text{B}_{12}\text{H}_{12}$. We performed these calculations with the VASP software [40] by following the generalized gradient approximation to the exchange-correlation energy due to Perdew *et al.* [41]. The projector augmented-wave method was used to represent the ionic cores [42], and the electronic states $1s\text{-}2s$ Li, $1s\text{-}2s\text{-}2p$ B and $1s$ H were considered as valence. Wave functions were represented in a plane-wave basis set truncated at 650 eV. By using these parameters and dense \mathbf{k} -point grids for Brillouin zone integration, the resulting energies were converged to within 1 meV per formula unit. In the geometry relaxations, a tolerance of $0.01 \text{ eV}\cdot\text{\AA}^{-1}$ was imposed on the atomic forces.

Ab initio molecular dynamics (AIMD) simulations based on DFT were carried out to assess the reliability of the interatomic potential model employed in the classical molecular dynamics simulations (Supplementary Fig.3 and Supplementary Discussion). The AIMD simulations were performed in the canonical (N, V, T) ensemble considering constant number of particles, volume and temperature. The constrained volumes were equal to the equilibrium volumes determined at zero temperature, thus we neglected possible thermal expansion effects. Nevertheless, in view of previous first-principles work [43], it is reasonable to expect that thermal expansion effects do not affect significantly the estimation of lithium diffusion coefficients at the considered temperatures. The temperature in the AIMD simulations was kept fluctuating around a set-point value by using Nose-Hoover thermostats. A large simulation box containing 832 atoms was employed in all the simulations, and periodic boundary conditions were applied along the three Cartesian directions. Newton's equations of motion were integrated by using the customary Verlet's algorithm and a time-step length of $\delta t = 10^{-3}$ ps. Γ -point sampling for integration within the first Brillouin zone was employed in all the AIMD simulations. The AIMD simulations comprised long simulation times of ~ 100 ps.

Estimation of key quantities. The mean square displacement of lithium ions was estimated with the formula [43]:

$$\text{MSD}_{\text{Li}}(\tau) = \frac{1}{N_{\text{ion}}(N_{\text{step}} - n_{\tau})} \times \sum_{i=1}^{N_{\text{ion}}} \sum_{j=1}^{N_{\text{step}} - n_{\tau}} |\mathbf{r}_i(t_j + \tau) - \mathbf{r}_i(t_j)|^2, \quad (1)$$

where $\mathbf{r}_i(t_j)$ is the position of the migrating ion i at time $t_j (= j \cdot \delta t)$, τ represents a lag time, $n_{\tau} = \tau/\delta t$, N_{ion} is the total number of mobile ions, and N_{step} the total number of time steps. The maximum n_{τ} was chosen equal to $N_{\text{step}}/2$, hence we could accumulate enough statistics to reduce significantly the fluctuations in $\text{MSD}_{\text{Li}}(\tau)$ at large τ 's. The diffusion coefficient of lithium ions then was obtained with the Einstein relation:

$$D_{\text{Li}} = \lim_{\tau \rightarrow \infty} \frac{\text{MSD}_{\text{Li}}(\tau)}{6\tau}, \quad (2)$$

by performing linear fits to the averaged MSD_{Li} values calculated at long τ .

The angular autocorrelation function of the closoborane $(\text{BH})_{12}^{2-}$ icosahedra was estimated according to the expression [23]:

$$\phi_{\text{B}_{12}\text{H}_{12}}(\tau) = \langle \hat{\mathbf{r}}(t) \cdot \hat{\mathbf{r}}(t + \tau) \rangle, \quad (3)$$

where $\hat{\mathbf{r}}$ is a unitary vector connecting the center of mass of each closoborane unit with one of its edges and

$\langle \dots \rangle$ denotes thermal average considering all the closoborane icosahedra. This autocorrelation function typically decays as $\propto \exp[-\lambda_{\text{B}_{12}\text{H}_{12}} \cdot \tau]$, where the parameter $\lambda_{\text{B}_{12}\text{H}_{12}}$ represents a characteristic reorientational frequency. When the $(\text{BH})_{12}^{2-}$ reorientational motion is significant, that is, $\lambda_{\text{B}_{12}\text{H}_{12}}$ is large, the $\phi_{\text{B}_{12}\text{H}_{12}}$ function decreases rapidly to zero with time.

Isothermal entropy changes associated with the barocaloric effect were estimated with the formula [2, 3]:

$$\Delta S(P, T) = - \int_0^P \left(\frac{\partial V}{\partial T} \right)_{P'} dP', \quad (4)$$

where P represents the maximum applied hydrostatic pressure and V the volume of the system. Likewise, the accompanying adiabatic temperature shift was calculated as:

$$\Delta T(P, T) = \int_0^P \frac{T}{C_{P'}(T)} \cdot \left(\frac{\partial V}{\partial T} \right)_{P'} dP', \quad (5)$$

where $C_P(T) = \left(\frac{dU}{dT} \right)_P$ is the heat capacity of the crystal obtained at constant pressure and temperature conditions.

In order to accurately compute the $\Delta S(P, T)$ and $\Delta T(P, T)$ shifts induced by pressure, we calculated the corresponding volumes and heat capacities over dense grids of (P, T) points spaced by $\delta P = 0.1$ GPa and $\delta T = 25$ K. Spline interpolations were subsequently applied to the calculated sets of points, which allowed for accurate determination of $(\partial V/\partial T)_P$ and heat capacities. The ΔS and ΔT values appearing in Fig.2d-e were obtained by numerically integrating those spline functions with respect to pressure.

DATA AVAILABILITY

The data that support the findings of this study are available from the corresponding author (C.C.) upon reasonable request.

ACKNOWLEDGEMENTS

C. C. acknowledges support from the Spanish Ministry of Science, Innovation and Universities under the "Ramón y Cajal" fellowship RYC2018-024947-I. D. E. acknowledges support from the Spanish Ministry of Science, Innovation and Universities under the Grant PID2019-106383GB-C41 and the Generalitat Valenciana under the Grant Prometeo/2018/123 (EFIMAT). Computational resources and technical assistance were provided by the Informatics Service of the University of Valencia through the Tirant III cluster and the Center for Computational Materials Science of the Institute for Materials Research, Tohoku University (MATERIAL science Supercomputing system for Advanced MULTIscale simulations towards NExt-generation-Institute of Material Research) (Project No-19S0010).

- [1] Mañosa, Ll. & Planes, A. Materials with Giant Mechanocaloric Effects: Cooling by Strength. *Adv. Mater.* **29**, 1603607 (2017).
- [2] Moya, X., Kar-Narayan, S. & Mathur, N. D. Caloric materials near ferroic phase transitions. *Nat. Mater.* **13**, 439 (2014).
- [3] Cazorla, C. Novel mechanocaloric materials for solid-state cooling applications. *Appl. Phys. Rev.* **6**, 041316 (2019).
- [4] Aznar, A., Lloveras, P., Barrio, M., Negrier, Ph., Planes, A., Ll. Mañosa, Mathur, N. D., Moya, X. & Tamarit, J.-Ll. Reversible and irreversible colossal barocaloric effects in plastic crystals. *J. Mater. Chem. A* **8**, 639 (2020).
- [5] Aznar, A., Lloveras, P., Romanini, M., Barrio, M., Tamarit, J. Ll., Cazorla, C., Errandonea, D., Mathur, N. D., Planes, A., Moya, X. & Mañosa, Ll. Giant barocaloric effects over a wide temperature range in superionic conductor AgI. *Nat. Commun.* **8**, 1851 (2017).
- [6] Li, B. *et al.* Colossal barocaloric effects in plastic crystals. *Nature* **567**, 506 (2019).
- [7] Lloveras, P., Aznar, A., Barrio, M., Negrier, Ph., Popescu, C., Planes, A., Ll. Mañosa, Stern-Taulats, E., Avramenko, A., Mathur, N. D., Moya, X. & Tamarit, J.-Ll. Colossal barocaloric effects near room temperature in plastic crystals of neopentylglycol. *Nat. Commun.* **10**, 1803 (2019).
- [8] Sagotra, A. K., Errandonea, D. & Cazorla, C. Mechanocaloric effects in superionic thin films from atomistic simulations. *Nat. Commun.* **8**, 963 (2017).
- [9] Sagotra, A. K. & Cazorla, C. Stress-mediated enhancement of ionic conductivity in fast-ion conductors. *ACS Appl. Mater. Interfaces* **9**, 38773 (2017).
- [10] Hull, S. Superionics: crystal structures and conduction processes. *Rep. Prog. Phys.* **67**, 1233 (2004).
- [11] C. Cazorla & Errandonea, D. Giant mechanocaloric effects in fluorite-structured superionic materials. *Nano Lett.* **16**, 3124 (2016).
- [12] Sagotra, A. K., Chu, D. & Cazorla C. Room-temperature mechanocaloric effects in lithium-based superionic materials. *Nat. Commun.* **9**, 3337 (2018).
- [13] Min, J., Sagotra, A. K. & Cazorla, C. Large barocaloric effects in thermoelectric superionic materials. *Phys. Rev. Mater.* **4**, 015403 (2020).
- [14] Cazorla, C. Refrigeration based on plastic crystals. *Nature* **567**, 470 (2019).
- [15] Her, J.-H., Yousufuddin, M., Zhou, W., Jalisatgi, S. S., Kulleck, J. G., Zan, J. A., Hwang, S.-J., Bowman, R. C. & Udovic, T. J. Crystal structure of $\text{Li}_2\text{B}_{12}\text{H}_{12}$: A possible intermediate species in the decomposition of LiBH_4 . *Inorg. Chem.* **47**, 9757 (2008).
- [16] Lai, Q., Sun, Y., Modi, P., Cazorla, C., Demirci, U. B., Ares, J. R., Leardini, F. & Aguey-Zinsou, K. F. How to design hydrogen storage materials? Fundamentals, synthesis, and storage tanks. *Adv. Sustainable Syst.* **3**, 1900043 (2019).
- [17] Shevlin, S. A., Cazorla, C. & Guo, Z. X. Structure and defect chemistry of low and high temperature phases of LiBH_4 . *J. Phys. Chem. C* **116**, 13488 (2012).
- [18] Paskevicius, M., Pitt, M. P., Brown, D. H., Sheppard, D. A., Chumphongphan, S. & Buckley, C. E. First-order phase transition in the $\text{Li}_2\text{B}_{12}\text{H}_{12}$ system. *Phys. Chem. Chem. Phys.* **15**, 15825 (2013).
- [19] Luo, X., Rawal, A., Cazorla, C. & Aguey-Zinsou, K. F. Facile self-forming superionic conductors based on complex borohydrides surface oxidation. *Adv. Sustainable Syst.* **4**, 1900113 (2020).
- [20] Mohtadi, R. & Orimo, S. I. The renaissance of hydrides as energy materials. *Nat. Rev. Mater.* **2**, 16091 (2016).
- [21] Udovic, T. J., Matsuo, M., Unemoto, A., Verdal, N., Stavila, V., Skripov, A. V., Rush, J. J., Takamura, H. & Orimo, S.-I. Sodium superionic conduction in $\text{Na}_2\text{B}_{12}\text{H}_{12}$. *Chem. Commun.* **50**, 3750 (2014).
- [22] Jorgensen, M., Shea, P. T., Tomich, A. W., Varley, J. B., Bercx, M., Lovera, S., Cerny, R., Zhou, W., Udovic, T. J., Lavallo, V., Jensen, T. R., Wood, B. C. & Stavila, V. Understanding Superionic Conductivity in Lithium and Sodium Salts of Weakly Coordinating Closo-Hexahalocarborate Anions. *Chem. Mater.* **32**, 1475 (2020).
- [23] Sau, K., Ikeshoji, T., Kim, S., Takagi, S., Akgi, K. & Orimo, S.-i. Reorientational motion and Li^+ ion transport in $\text{Li}_2\text{B}_{12}\text{H}_{12}$ system: Molecular dynamics study. *Phys. Rev. Mater.* **3**, 075402 (2019).
- [24] Skripov, A. V., Soloninin, A. V., Ley, M. B., Jensen, T. R. & Filinchuk, Y. Nuclear magnetic resonance studies of BH_4 reorientations and Li diffusion in $\text{LiLa}(\text{BH}_4)_3\text{Cl}$. *J. Phys. Chem. C* **117**, 14965 (2013).
- [25] Stern-Taulats, E., Planes, A., Lloveras, P., Barrio, M., Tamarit, J.-Ll., Pramanick, S., Majumdar, S., Yüce, S., Emre, B., Frontera, C. & Mañosa, Ll. Tailoring barocaloric and magnetocaloric properties in low-hysteresis magnetic shape memory alloys. *Acta Mater.* **96**, 324 (2015).
- [26] Stern-Taulats, E., Gracia-Condal, A., Planes, A., Lloveras, P., Barrio, M., Tamarit, J.-Ll., Pramanick, S., Majumdar, S. & Mañosa, Ll. Reversible adiabatic temperature changes at the magnetocaloric and barocaloric effects in $\text{Fe}_{49}\text{Rh}_{51}$. *App. Phys. Lett.* **107**, 152409 (2015).
- [27] Lloveras, P., Stern-Taulats, E., Barrio, M., Tamarit, J.-Ll., Crossley, S., Li, W., Pomjakushin, V., Planes, A., Mañosa, Ll., Mathur, N. D. & Moya, X. Giant barocaloric effects at low temperature in ferroelectric ammonium sulphate. *Nat. Commun.* **6**, 8801 (2015).
- [28] Bermúdez-García, J. M., Sánchez-Andújar, M., Castro-García, S., López-Beceiro, J., Artiaga, R. & Señaris-Rodríguez, M. A. Giant barocaloric effect in the ferroic organic-inorganic hybrid $[\text{TPrA}][\text{Mn}(\text{dca})_3]$ perovskite under easily accessible pressures. *Nat. Commun.* **8**, 15715 (2017).
- [29] Bermúdez-García, J. M., Sánchez-Andújar, M. & Señaris-Rodríguez, M. A. A new playground for organic-inorganic hybrids: Barocaloric materials for pressure-induced solid-state cooling. *J. Phys. Chem. Lett.* **8**, 4419 (2017).
- [30] Gorev, M., Bogdanov, E., Flerov, I. N. & Laptash, N. M. Thermal expansion, phase diagrams and barocaloric effects in $(\text{NH}_4)_2\text{NbOF}_5$. *J. Phys.: Condens. Matter* **22**, 185901 (2010).
- [31] Rodriguez, E. L. & Filisko, F. E. Thermoelastic temperature changes in poly(methyl methacrylate) at high hydrostatic pressure: Experimental. *J. Appl. Phys.* **53**, 6536 (1982).

- [32] Vallone, S. P., Tantillo, A. N., dos Santos, A. M., Molaison, J. J., Kulmaczewski, R., Chapoy, A., Ahmadi, P. Halcrow, M. A., & Sandeman, K. G. Giant barocaloric effect at the spin crossover transition of a molecular crystal. *Adv. Mater.* **31**, 1807334 (2019).
- [33] Tang, W. S., Unemoto, A., Zhou, W., Stavila, V., Matsuo, M., Wu, H., Orimo, S.-I. & Udovic, T. J. Unparalleled lithium and sodium superionic conduction in solid electrolytes with large monovalent cage-like anions. *Energy Environ. Sci.* **8**, 3637 (2015).
- [34] Kim, S., Oguchi, H., Toyama, N., Sato, T., Takagi, S., Otomo, T., Arunkumar, D., Kuwata, N., Kawamura, J. & Orimo, S.-I. A complex hydride lithium superionic conductor for high-energy-density all-solid-state lithium metal batteries. *Nat. Commun.* **10**, 1081 (2019).
- [35] Verdal, N., Wu, H., Udovic, T. J., Stavila, V., Zhou, W. & Rush, J. J. Evidence of a transition to reorientational disorder in the cubic alkali-metal dodecahydro-closo-dodecaborates. *J. Solid State Chem.* **184**, 3110 (2011).
- [36] Christy, A. G. Isosymmetric structural phase transitions: Phenomenology and examples. *Acta Cryst.* **B51**, 753 (1995).
- [37] Adams, D. M., Hatton, P. D., Heath, A. E. & Russell, D. R. X-ray diffraction measurements on potassium nitrate under high pressure using synchrotron radiation. *J. Phys. C: Solid State Phys.* **21**, 505 (1988).
- [38] Plimpton, S. J. Fast parallel algorithms for short-range molecular dynamics. *J. Comp. Phys.* **117**, 1 (1995) <http://lammmps.sandia.gov>.
- [39] Cazorla, C. & Boronat, J. Simulation and understanding of atomic and molecular quantum crystals. *Rev. Mod. Phys.* **89**, 035003 (2017).
- [40] Kresse, G. & Furthmüller, J. Efficient iterative schemes for ab initio total-energy calculations using a plane-wave basis set. *Phys. Rev. B* **54**, 11169 (1996).
- [41] Perdew, J. P., Burke, K. & Ernzerhof, M. Generalized gradient approximation made simple. *Phys. Rev. Lett.* **77**, 3865 (1996).
- [42] Blöchl, P. E. Projector augmented-wave method. *Phys. Rev. B* **50**, 17953 (1994).
- [43] Sagotra, A. K., Chu, D. & Cazorla, C. Influence of lattice dynamics on lithium-ion conductivity: A first-principles study. *Phys. Rev. Mater.* **3**, 035405 (2019).

AUTHOR CONTRIBUTIONS

K.S. and C.C. conceived the study and planned the research. K.S. performed the molecular dynamics simulations and C.C. the first-principles calculations and barocaloric analysis. Results were discussed by all the authors. All the authors participated in the writing of the manuscript.

ADDITIONAL INFORMATION

Supplementary information is available in the online version of the paper.

COMPETING INTERESTS

The authors declare no competing interests.